Journal of Materials Chemistry C

ROYAL SOCIETY OF CHEMISTRY

PAPER

View Article Online
View Journal | View Issue

Cite this: J. Mater. Chem. C, 2021, 9, 9619

Flexible thermosensitive films based on shallow-trap persistent luminescence for high-resolution texture imaging of fingerprints even through latex gloves†

Shenghui Zheng,[ab] Junpeng Shi,[c] Xiaodan Wang,[ab] Xiaoyan Fu,*[d] Hongyong Fan[ab] and Hongwu Zhang *[ae]

Received 23rd April 2021,
Accepted 21st June 2021

DOI: 10.1039/d1tc01888d

rsc.li/materials-c

Here, we have developed a novel thermosensitive technique based on shallow-trap persistent luminescence to achieve high-resolution and long-duration texture imaging of fingerprints even through latex gloves. A thermosensitive flexible film that consists of a transparent silica gel embedded with a shallow-trap $Bi_2Ga_4O_9:Eu^{3+},Cr^{3+}$ (BGO) phosphor microarray exhibits broadband near-infrared PersL, which enables sensitive temperature sensing using a thermally stimulated luminescence (TSL) method. The uniform surface conical arrays of the BGO film ensure a high thermal sensing resolution. Only a simple touch is enough to induce thermal distribution that can be easily visualized as luminescence using an EMCCD camera. Furthermore, the BGO film responds rapidly to small temperature fluctuations with high sensitivity (8.10 ± 0.476% K^{-1}), enabling fingerprint imaging even through latex gloves in only a few seconds. This imaging strategy is very promising for sensitive temperature sensing without power supply, and it also opens new application opportunities for shallow-trap PersL materials.

Introduction

Owing to the unique individual finger patterns, fingerprint detection is an important and effective identification technique widely applied in criminal investigation, signature identification, and security verification.[1] Many methods and contrast agents were explored to obtain high-resolution fingerprints.[2–7] Currently, fingerprint identification is a reliable, direct and efficient identification technique. Its outstanding performance is indispensable in different areas, and it is accepted as a piece of final evidence for many severe criminal cases. However, most studies focus on the physical characteristics and heterogenous chemical components. Although detection by these imaging strategies has many advantages, they still suffer from a main drawback, namely all of them are based on sweat mingled chemicals and metabolites, need intrinsic (sweat, sebum) or extrinsic (dirt, grease) constituents.[8,9] Many crimes are committed with gloves to avoid potential fingerprint identification, and therefore the standard fingerprint detection techniques fail to provide clear and valid fingerprints, which inevitably limit their final use. Thus, the development of novel shielded fingerprint detection techniques to resolve this problem is of utmost importance.

As is well known, trapped electrons of PersL phosphors can be released in a controlled manner using external thermal or optical stimulation, yielding the corresponding luminescence intensity. This property can be employed for temperature sensing, optical data storage, and *in vivo* imaging.[10–12] Usually, the performance of trap-related PersL sensors are determined by the trap depth. Zhuang *et al.* have recently demonstrated that deep-trap PersL materials $(Sr_{1-x}Ba_x)Si_2O_2N_2:Eu/Yb,Dy$ can be applied in optical data storage.[13,14] Smet *et al.* reported a stress recording method by electrons reshuffling toward deep-trap and readout by optical stimulation.[15] The well-known PersL materials with traps of an intermediate depth exhibited optimal duration and intensity (*e.g.* $LiGa_5O_8:Cr^{3+}$ and $ZnGa_2O_4:Cr^{3+}$), and they were widely used for background-free *in vivo* imaging.[16,17] In contrast, the electrons in shallow traps

[a] Key Lab of Urban Pollutant Conversion, Institute of Urban Environment, Chinese Academy of Sciences, Xiamen, 361021, China. E-mail: hwzhang@iue.ac.cn
[b] University of Chinese Academy of Sciences, No. 19A Yuquan Road, Beijing 100049, China
[c] Key Laboratory of Design and Assembly of Functional Nanostructures, Fujian Institute of Research on the Structure of Matter, Chinese Academy of Sciences, Fuzhou 350002, China
[d] College of Materials Science and Engineering, Key Laboratory of Functional Materials and Applications of Fujian Province, Xiamen University of Technology, Xiamen 361024, China. E-mail: fuxiaoyan@xmut.edu.cn
[e] School of Chemistry and Material Sciences, Ludong University, Yantai 264025, China

† Electronic supplementary information (ESI) available: Rietveld refinement XRD pattern, PersL decay curves, and different fingerprint detection results with latex gloves. See DOI: 10.1039/d1tc01888d

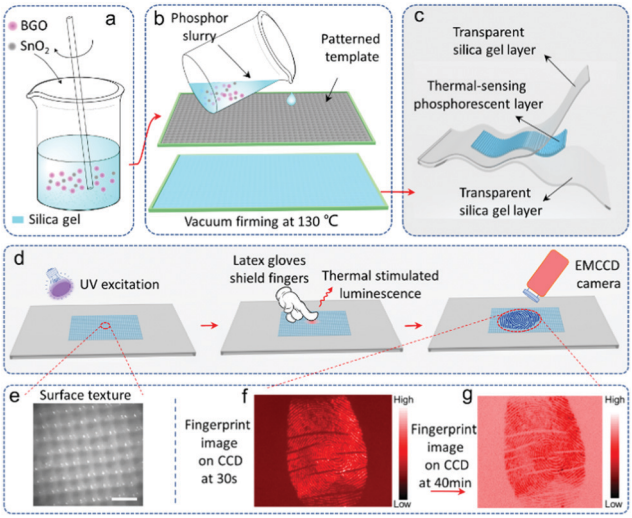

Fig. 1 Preparation of a phosphor film and its application in fingerprint detection. (a) Mixing of BGO phosphor powder with transparent silica gel precursors. (b) Pouring the phosphor slurry onto a patterned template and vacuum firming at 130 °C for 30 min. (c) Schematic configuration of BGO film with two transparent silica gel layers. (d) Fingerprint detection process based on thermal stimulated luminescence. (e) Optical microscopy image of the film surface texture. The scale bar is 200 μm. (f) and (g) Fingerprint images on an EMCCD camera taken at 30 s and 40 min after finger touching.

have a low potential barrier so that they can be quickly excited. This may yield the corresponding luminescence signals even under low thermal fluctuations, which is favorable for the precise measurement of small temperature changes.[18,19] Based on this theory, we have designed a novel thermosensitive technique based on shallow-trap PersL for high-resolution texture imaging of fingerprints even through latex gloves. When a finger in latex gloves touches the surface of the thermosensitive PersL film, the heat can be briefly transferred to the film through the latex glove, inducing the temperature rise of the covered area. Simultaneously, thermally stimulated luminescence (TSL) can be produced, and electrons in the shallow trap will be consumed. In this way, the fingerprint information can be displayed and stored on the thermosensitive PersL luminescent film (Fig. 1).

The critical problem of this novel fingerprint detection technique was the development of suitable shallow trap related PersL materials. In this paper, we have developed near-infrared (NIR) PersL phosphors with a trap depth of 0.65 eV, which have shown excellent thermosensitive luminescence properties. A flexible thermosensitive NIR luminescent film that provided a good finger touching surface was prepared by mixing with transparent silica gel. Due to excellent thermosensitive PersL properties, the BGO film can easily display and store high-resolution fingerprint information. Furthermore, the fingerprint cannot be seen by the naked eye because of the NIR TSL, which may help to protect the private aspect. At the same time, the high-resolution fingerprint, even when secured by latex gloves, can be visualized using an Electron-Multiplying CCD (EMCCD) camera, suggesting its outstanding identification ability.

Experimental

Materials synthesis

$Bi_{2-x}Ga_{4-y}O_9$:xEu^{3+},yCr^{3+} (x = 0.25–3%; y = 0.25–2%) were prepared using two-step-sintering reaction method. Stoichiometric raw materials Bi_2O_3 (Aladdin, 99.99%), Ga_2O_3 (Aladdin, 99.99%), Eu_2O_3 (Aladdin, 99.99%), and $Cr(NO_3)_3{\cdot}9H_2O$ (Aladdin, 99.99%) were mixed and fully ground in an agate mortar. Then they were transferred to an alumina crucible and heated to 450 °C for 1 h in a muffle furnace. After cooling to room temperature, the precursors were ground again and sintered at 950 °C for 2 h in air atmosphere. Finally, shallow-trap persistent luminescence phosphors were obtained.

Preparation of phosphor containing films

The as prepared phosphor was ball-milled for 2 h, and then shifted through a 325 mesh sieve. The obtained fine phosphor powder was homogeneously mixed with nano-SnO_2 (Aladdin, 70–90 nm) and transparent silicone precursors (Aokai Co. Ltd) in a weight ratio of 1.2 : 0.2 : 1, the mixture was poured into a rectangle mold with conical groove arrays and then put in a vacuum drying oven at 130 °C for 30 min. After the curing process, a surface conical array film with an average thickness of 0.3 mm was obtained. Finally, the film was coated with two other transparent silica gel layers, using another curing process for 30 min in air to form an elastic BGO film.

Measurements and characterization

The powder X-ray diffraction (XRD) patterns of $Bi_{2-x}Ga_{4-y}O_9$:xEu^{3+},yCr^{3+} (x = 0.25–3%; y = 0.25–2%) were recorded on an X-ray diffractometer (X'Pert PRO, PANalytical) operated at 40 kV and 40 mA with Cu Kα (λ = 0.154 nm) radiation at a step size of 0.02°. PL and PLE spectra, afterglow curves, PersL decay curves, thermo-stimulated decay curves were recorded on a steady-state/transient fluorescence spectrophotometer (FLS 920, Edinburgh Instruments) equipped with a 450 W xenon lamp. ThL glow curves were recorded on a liquid nitrogen bath cryostat (OptistatDN-V2, Oxford Instruments) in a temperature range of 273–500 K with a heating rate of 10 K min^{-1}. Prior to the measurements, the sample was preirradiated with a 254 nm Hg lamp (6 W, Philips) for 2 min. Thermally stimulated decay curves were measured using a temperature controller (Intelligent temperature controller, Oxford Instruments). Images of the powder samples and BGO films in daylight were acquired using a complementary metal oxide semiconductor camera (D7000, Nikon). Afterglow images of BGO films were acquired using a cooled EMCCD camera (iXon, Andor), and a digital thermometer (ETS-D5, IKA) was used for contrast temperature indication during the measurements. All the measurements except XRD and ThL were performed at 295 K.

Results and discussion

Crystal structure and luminescence characterization of BGO

To obtain a shallow-trap PersL material suitable for a thermosensitive luminescent film, we synthesized a series of Eu^{3+} and

Cr^{3+} doped bismuth gallates using a solid-state route. The as-prepared BGO has a general formula of $Bi_{2-x}Ga_{4-y}O_9$:xEu^{3+},yCr^{3+} (x = 0.25–3%; y = 0.25–2%). X-Ray diffraction patterns (Fig. 2a and Fig. S1, ESI†) indicate that all the samples crystallized as pure orthorhombic $Bi_2Ga_4O_9$ with the Pbam space group (JCPDS #01-076-2240).[20] The increase of doping concentration does not yield any impurity phases, implying a good distribution of ions in the host material. In a typical crystal structure of BGO, there are two inequivalent Ga^{3+} sites and one Bi^{3+} site. The cell parameters of doped BGO are smaller than those of the undoped one (Table S1, ESI†), demonstrating that the Eu^{3+} (r = 0.947 Å, coordination number (CN) = 6) and Cr^{3+} (r = 0.615 Å, CN = 6) ions introduced are expected to occupy Bi^{3+} (r = 1.03 Å, CN = 6) and Ga^{3+} (r = 0.62 Å, CN = 6) ion sites, respectively, because of the similar ionic radii (Fig. 2b).[21]

The BGO phosphor exhibits good NIR photoluminescence (PL) properties (Fig. 2c). Its excitation spectrum upon monitoring at 706 nm consists of three prominent excitation bands located at 340, 445, and 620 nm, which correspond to $^4A_2 \rightarrow {}^4T_1(te^2)$, $^4A_2 \rightarrow {}^4T_1(t^2e)$, and $^4A_2 \rightarrow {}^4T_2(t^2e)$ transitions of Cr^{3+}, respectively.[22] Under UV (254 nm) and red light (620 nm) excitation, the emission spectra show a narrow band at 706 nm originating from the spin–forbidden $^2E \rightarrow {}^4A_2$ transitions and a broad NIR emission band at 736 nm from the spin-allowed $^4T_2(^4F) \rightarrow {}^4A_2$ transitions of Cr^{3+} ions.[23–25] Furthermore, the BGO sample exhibits NIR PersL properties under exposure to 254 nm UV light irradiation for 2 min (Fig. 2d), while the optimal PersL intensity is obtained when the Cr^{3+} concentration reaches 1% (Fig. S2, ESI†). At the same time, the PersL intensity can also be significantly enhanced by Eu^{3+} co-doping, and the best results are obtained for the Eu^{3+} concentration of 2% (inset in Fig. 2d). Thus, the BGO co-doped with 2% Eu^{3+} and 1% Cr^{3+} samples were chosen to prepare a finger-touching film by mixing it with transparent silica gel. After exposure to 254 nm for 2 min, the patterns containing the BGO phosphor persist for more than 20 min as monitored using an EMCCD camera (Fig. 2f). Furthermore, the BGO–silica film shows softness and excellent flexibility (Fig. 2g-i), which may provide an excellent finger-touching surface. The PersL spectrum of the BGO–silica film (Fig. 2e) is consistent with the PL spectrum, suggesting that both PersL and PL originate from the energy transition of Cr^{3+} ions. In a prolonged decay time over 20 min, the distinct NIR signals are also detectable using an EMCCD camera (Fig. 2g-ii). The above results suggest that the as-prepared BGO film possesses good NIR PersL properties and also provides flexibility and a soft surface.

Investigation of the trap depth distribution and the TSL mechanism

To further assess the potential of BGO film as temperature sensor, we measured the PersL properties in the range of 290–310 K (Fig. 3a). The PersL intensity of the BGO film surface significantly enhances from 650 to 820 nm. Fig. 3b depicts the

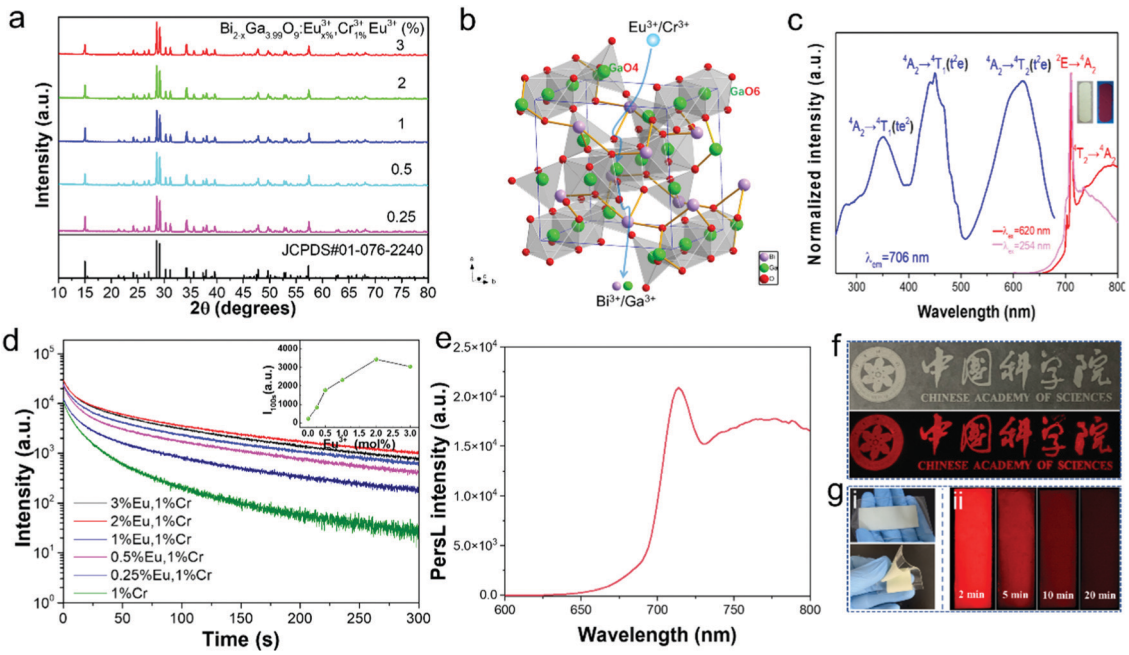

Fig. 2 (a) X-Ray diffraction patterns of the BGO samples; the standard BGO diffraction is referenced to the Joint Committee on Powder Diffraction Standards (JCPDS #01-076-2240). (b) The BGO unit cell and the coordinated polyhedron, Eu^{3+} and Cr^{3+} ions are incorporated at Bi^{3+} and Ga^{3+} sites, respectively. (c) Normalized excitation (blue line) and emission (red and purple lines) spectra of the representative $Bi_{1.98}Ga_{3.99}O_9$:2%Eu^{3+},1%Cr^{3+} sample. The inset shows the sample under daylight and UV irradiation. (d) PersL decay curves of BGO with different Eu^{3+} concentrations after 2 min of irradiation with 254 nm. The power density is 200 mW cm^{-2}. (e) The BGO PersL spectrum after 2 min of irradiation with 254 nm. (f) Photographs of the BGO mixture with transparent ink printed on paper under natural light (the upper panel) and PersL image after 254 nm (the lower panel) excited for 2 min. (g) Photographs of the BGO phosphor embedded in transparent silica gel film (i) and its PersL images after UV excitation at 254 nm for 2 min at different intervals (ii).

temperature dependence of the PersL integrated intensity of the BGO film, which is nearly proportional to the applied thermal stimulation. Notably, the calculated relative TSL sensitivity in the physiological temperature range is 8.10 ± 0.476% K^{-1}, suitable for thermal detection applications.[26,27]

The TSL behavior of the PersL phosphors was determined by the properties of traps that exist in these materials. Usually, the existence of numerous shallow traps with a narrow distribution is generally indispensable to detect small temperature fluctuations induced by finger touching. Here, we utilize thermoluminescence (ThL) to explore the trapping behavior of the BGO sample. The resultant energy levels of trap depths were calculated according to eqn (1).[28,29]

$$\frac{\beta E_{\mathrm{Trap}}}{kT_{\mathrm{m}}^2} = s\exp\left(\frac{E_{\mathrm{Trap}}}{kT_{\mathrm{m}}}\right) \quad (1)$$

here, β denotes the constant heating rate, E_{trap} is the trap depth, T_{m} is the maximum peak temperature of the ThL glow curve, k is the Boltzmann constant 8.617×10^{-5} (eV K^{-1}), and s is the frequency factor.

The ThL results show two broad peaks in the spectral profile, suggesting the existence of shallow and deep-trap levels in the BGO phosphor. Remarkably, doping with Eu^{3+} ions can increase the shallow-trap density (with the maximal density at 0.65 eV), and it significantly reduces the deep-trap density (0.87 eV) (Fig. 3c), greatly enhancing the PersL intensity and duration time (Fig. S3, ESI†). In the present case, without external light excitation, the ThL intensity gradually reduces following the decay time (Fig. 3d). Indeed, the electrons are gradually released from the shallow-trap because of the thermally assisted de-trapping process.[30,31] The additional temperature increase would facilitate this process, leaving fewer electrons in the shallow trap at the end of the heating. Thus, the ThL curves show lower intensity than those obtained without the thermal stimulation in the same delay time (inset of Fig. 3d, 20 min and 40 min). Consequently, the shallow-trap occupation decreases by about 40% and 36% for 20 and 40 min after the thermal stimulation. The decreasing tendency can be observed more clearly when following the ThL curve ratio (Fig. 3e). As the application of heat leads to charge release, the most dominant effect temperature shows a distribution peak at ~300 K, much closer to the body surface temperature. Thus, it implies that the low-temperature TSL properties of BGO are due to the thermal stimulation that acts on the shallow-trap levels.

Based on the above results and analysis, a schematic diagram of the TSL mechanisms in the BGO is proposed (Fig. 3f). In the BGO PersL phosphor, the trap levels are mainly distributed over an energy range at a shallow depth with Eu^{3+} co-doping. Under UV light irradiation (254 nm), the ground state electrons of Cr^{3+} ions are excited to the $4T_1(te^2)$ level (i), and some excited electrons are subsequently captured by trapping centers *via* the conduction band (CB) of the host (ii).[32,33] After sufficient irradiation, the traps are filled with electrons.

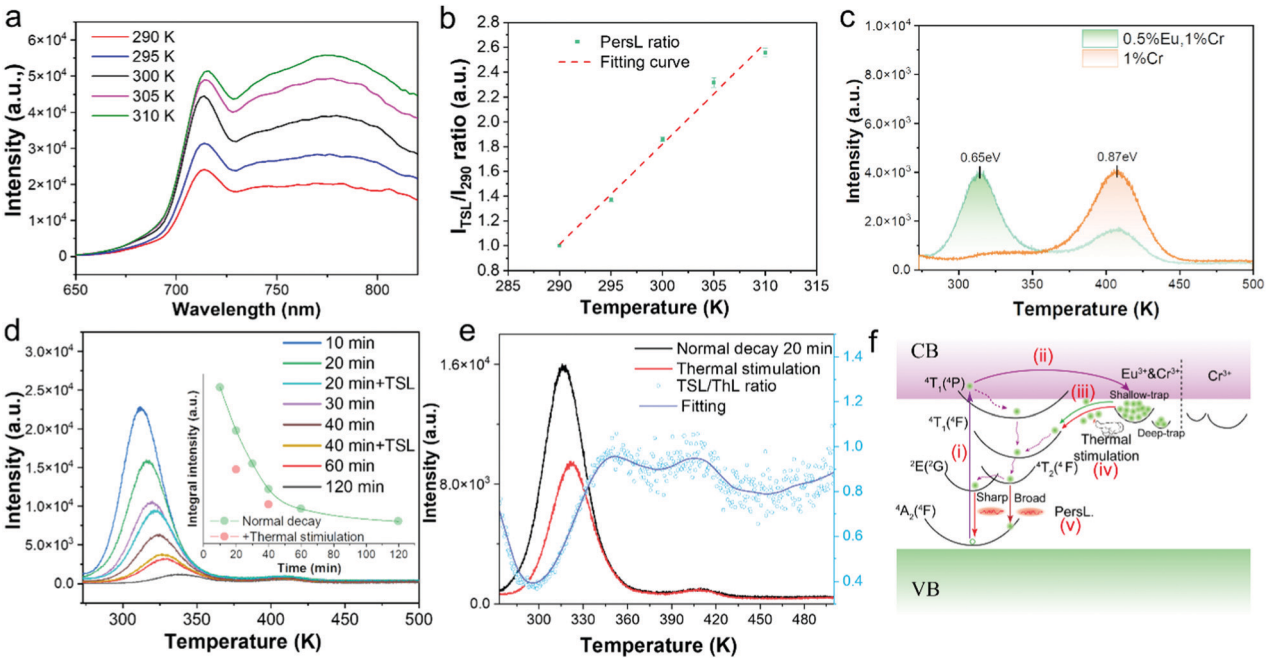

Fig. 3 (a) PersL spectra of the BGO film at various temperatures. (b) The ratio of the integrated PersL intensity to the initial intensity (I_{290}) of BGO under different thermal stimulations. Error bars were based on standard deviation (n = 3). (c) ThL glow curves of BGO at 10 min with and without Eu^{3+} co-doping. (d) A series of ThL glow curves for $Bi_{1.98}Ga_{3.99}O_9$:2%Eu^{3+},1%Cr^{3+} at different time intervals or accompanied by thermal stimulation. The inset shows the corresponding ThL integrated intensity. Before the ThL measurements, the sample was pre-irradiated under 254 nm for 2 min. The heating rate was 10 K min^{-1} for ThL measurements and 0.9 K s^{-1} for thermal stimulation, respectively. (e) The ThL glow curves with (red line) and without (black line) thermal stimulation after a 20 min delay. The blue dotted line represents the ratio of both curves. (f) Schematic diagram of the mechanisms behind the BGO PersL and TSL phenomena presented as a configurational coordinate diagram.

When the UV light excitation ceases, the recombination between the electrons released from shallow-trap levels and the ionized Cr^{3+} dominates the PersL process (iii).[34,35] In the present case, the thermal stimulation can promote the electron release efficiency (iv), providing different PersL intensities (v). Since the electrons in shallow traps of BGO can be quickly released at the body surface temperature to induce NIR luminescence, it is possible to utilize this behavior for thermal detection of high-resolution fingerprints.

TSL characteristics of the BGO film

Then, we investigated the TSL intensity to confirm the fingerprint detection capability of the BGO film. The thermal stimulation was performed in the heating stage, and the ambient temperature was maintained at 295 K to avoid the temperature fluctuation effect on the PersL intensity. Furthermore, we measured temperature transmission rate from a finger in latex gloves (Fig. 4a). The surface temperature of the touch point increases rapidly in the first 10 s. Subsequently, the temperature slowly increases and finally stabilizes at ~305 K (gray dotted line in Fig. 4a). The infrared thermal imaging further confirms that the film's surface temperature can reach ~303 K after touching for 10 s (Fig. 4c–e). Since it is difficult to simulate the temperature increase due to finger touching, a linear heating rate of 0.9 K s^{-1} in the range of 295–303 K

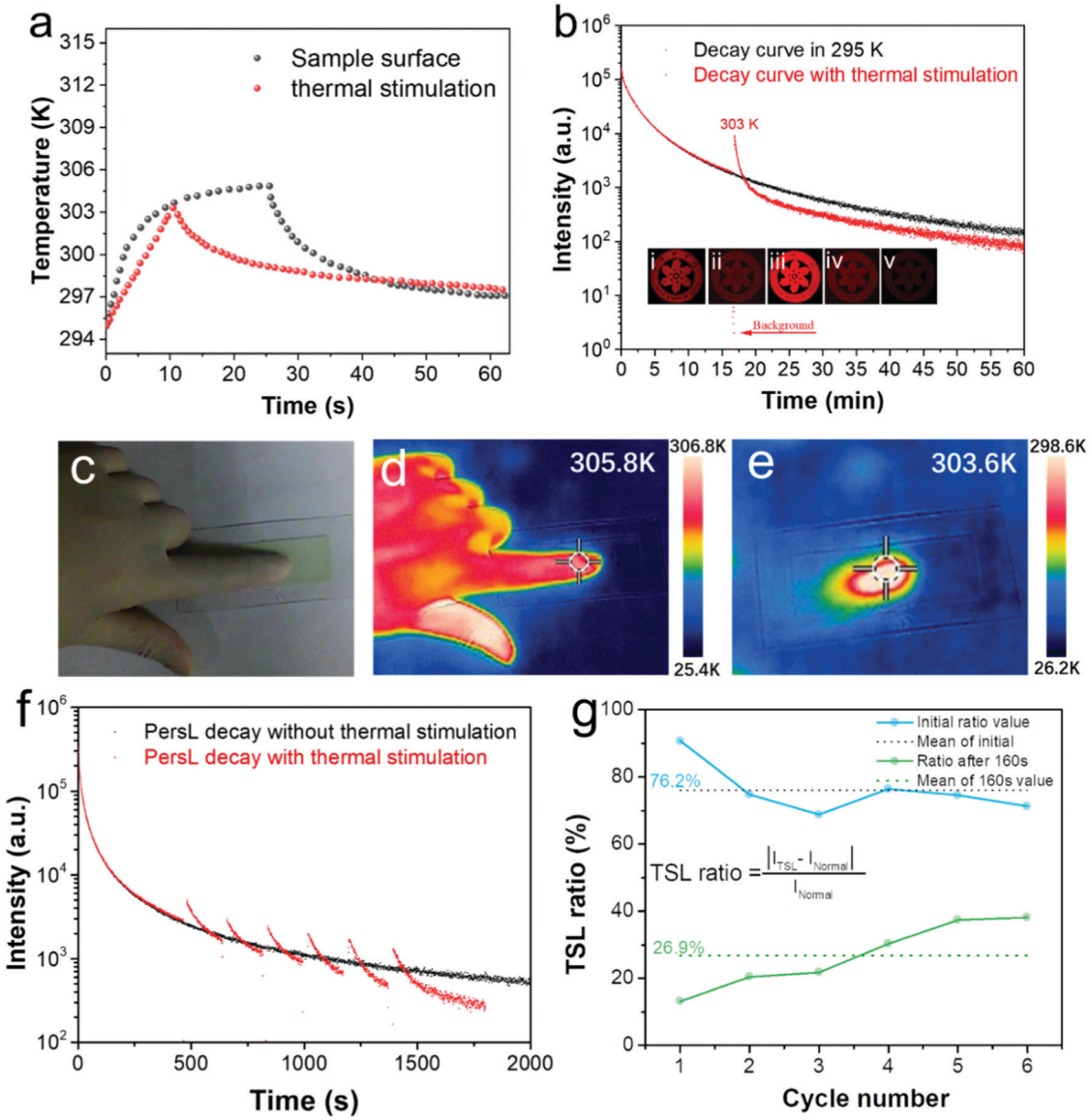

Fig. 4 (a) The thermal transmission curve from the finger to the BGO film surface during the touch process (gray dot line) and heating curve applied on the film during TSL measurements (red dot line). (b) Comparison of PersL decay curve with and without thermal stimulation for a long duration. The inset shows the PersL photos of the BGO pattern in the time points of 10, 15, 17, 18 and 20 min corresponding to the thermal stimulation decay curve. (c–e) The infrared thermal images under stimulation with latex gloves covered finger that are touching for 10 s. (f) Normal PersL decay curve (λ_{em} = 706 nm) of the $Bi_{1.98}Ga_{3.99}O_9$:2%Eu^{3+},1%Cr^{3+} at 295 K (black line). The persistent luminescence natural decay for 485 s and then under periodical thermal stimulation to 303 K at a heating rate of 0.9 K s^{-1} (red line). (g) Ratio of the surplus TSL intensity to the natural PersL decay intensity.

(red dotted line in Fig. 4a) replaced the surface temperature fluctuation to investigate TSL properties after the finger touching. After a sufficient decay time (16 min), the temperature increase (to 303 K) induces an intense burst of the decay PersL intensity, which is about 1.9 times higher than that of the normal decay curve. This burst emission can easily be detected *via* an EMCCD camera (inset in Fig. 4b-iii), suggesting that the finger-touching area can also be visualized, and unmistakable temperature increase can be obtained depending on the sensitive TSL properties. More importantly, the following decay intensity of the temperature-increased area is slightly weaker (0.8 times of the normal decay curve at 36 min) than that of other areas (Fig. 4b). The apparent difference in the PersL intensity can persist for a longer time. It can also be recorded by an EMCCD camera (inset in Fig. 4bi–v), indicating that the fingerprint information may be stored for a prolonged duration. Furthermore, the TSL intensity's dependency on the thermal stimulation cycles show similar decay behavior under repeated stimulations (Fig. 4f), implying that the temperature detection can be conducted many times on the BGO film after the UV excitation. For a single UV excitation, the intensity values gradually decrease with the number of thermal stimulation cycles. As presented in Fig. 4g, the contribution of the thermally induced PersL intensity is 90.6% higher than that of the normal decay curve. It decreases to an average of 76.2% after five stimulation cycles. However, this ratio value shows an increasing tendency after 160 s. It increases from 13% to 36%, with an average of 26.9% after five stimulation cycles. These experiments reveal that the TSL is driven by a thermally activated electron transition, showing a distinct intensity change within the range of body temperature fluctuations and demonstrating its potential applications for highly sensitive thermal sensors.

TSL driving fingerprint detection of the BGO film

The above results reveal that the BGO film is highly sensitive for thermal detection above the ambient temperature (295 K). Herein, we have imaged a real-time luminescence of the film area covered by a finger in a latex glove (thickness at finger ~0.09 mm) using an EMCCD camera (Fig. 5a) to demonstrate the fingerprint detection performance of the BGO film. After only 4 s (~301 K) of the touching duration, a high-resolution fingerprint image is obtained. The fingerprint can be distinguished even if the finger is covered by latex gloves (Fig. 5b and c) because the finger patterns induce the temperature fluctuation of the contact film surface. Different TSL intensities of the film appeared in the pattern area. This fingerprint detection technique does not require the remains of sweat or sebum liquid residuals, which differs from those of the commonly used fingerprint detection methods.[36–38] The BGO PersL film

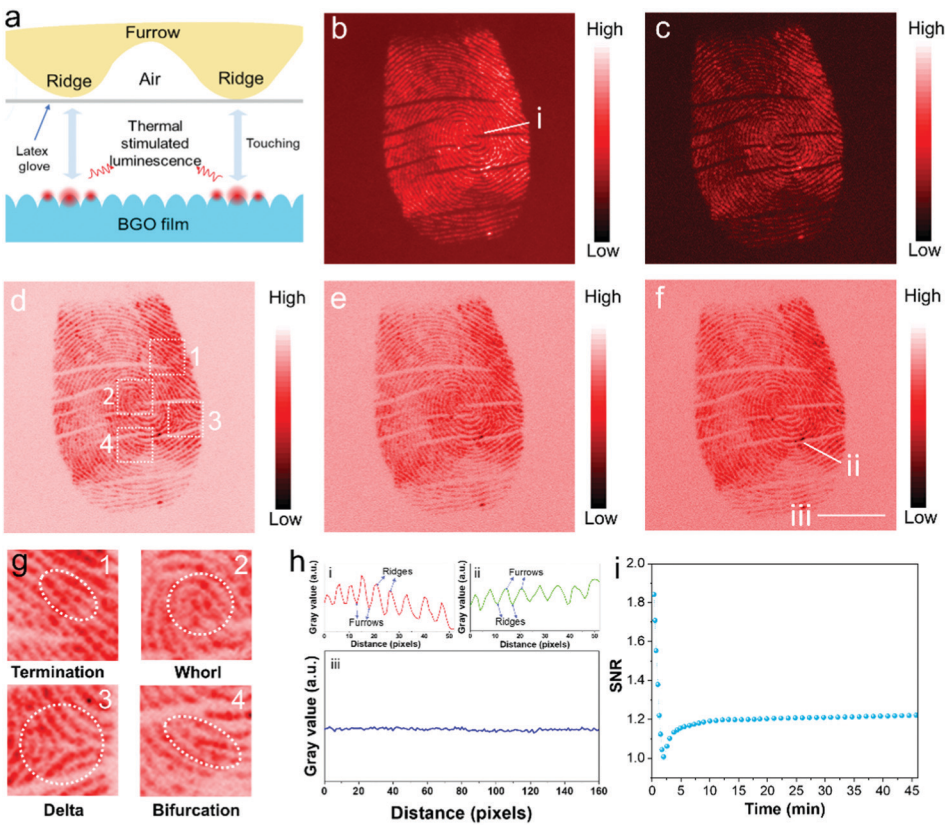

Fig. 5 (a) Schematic illustration of TSL-mediated imaging of fingerprints. (b–f) The detection results of fingerprints covered by latex gloves. The images were taken at 30 s, 60 s, 10 min, 20 min, and 40 min after finger touching. (g) The corresponding magnified images of selected area from (d). (h) The gray value variation shown from white line in (b) and (f). (i) The signal to noise ratio values under different duration times after finger touching for 4 s.

can provide a clear fingerprint pattern with improved separation between the ridges and furrows compared to the common method when latex gloves are used (Fig. S4, ESI†), and it also shows a clearer pattern compared with the smooth film without surface conical arrays (Fig. S5, ESI†). More importantly, since the TSL process consumes a large number of electrons in the shallow trap, the afterglow intensity of the film's fingerprint area is weaker than that in other areas, which can be clearly recorded using an EMCCD camera. Even 40 min later, the fingerprint can still be detected as a negative image pattern (Fig. 5d–f). In this way, long-lasting fingerprint detection and storage are achieved without a power supply and "indirect contact" using this novel technique. Meanwhile, the detailed information of the fingerprints including termination, whorls, deltas and bifurcation, could be easily recognized in high-magnification images (Fig. 5g). The variation in the gray value across the fingerprint is shown in Fig. 5h from the white line in Fig. 5b and f. The value changes a little without thermal stimulation (Fig. 5h-iii). In contrast, significant variation occurs after the finger touching (Fig. 5h-i and ii). The signal to noise ratio (SNR) between the contact area and the non-contact background is stable for more than 45 min (Fig. 5i), showing a satisfactory value above the EMCCD sensitivity ($\sim$1.1) in the maximum duration. Thus, the above results reveal that the BGO film possesses good thermal sensitivity, and it can successfully visualize latex glove shielded fingerprints on the basis of the TSL spatial difference on the contact surface.

Conclusions

In summary, we demonstrated the successful synthesis of the flexible BGO-based film with near-infrared persistent luminescence. The film could be efficiently used for sensitive thermal sensing and high-resolution visualization, which was contributed by the phosphor's shallow-trap distribution and conical surface arrays. Thermal stimulation luminescence played a key role in temperature sensing. A quick response of the persistent luminescence intensity to the thermal stimulation, and its misalignment with the unstimulated one, could be observed using an EMCCD camera for a long duration. Interestingly, the thermal distribution of the finger patterns could be easily visualized in the form of luminescence by a simple touch for a few seconds, even latex gloves protected the fingerprint. Through the method of thermal stimulation, the long time fingerprint detection purpose without power supply and "indirect contact" has been realized suggesting a new application concept of shallow-trap materials.

Conflicts of interest

There are no conflicts to declare.

Acknowledgements

This work was supported by the National Natural Science Foundation of China (11974013 and 61705228) and the Key Program of International Cooperation of Fujian Province (2018I0018 and 2019I0032).

References

1 K. Song, P. Huang, C. Yi, B. Ning, S. Hu, L. Nie, X. Chen and Z. Nie, *ACS Nano*, 2015, **9**, 12344–12348.
2 Z. Lei, X. Ling, Q. Mei, S. Fu, J. Zhang and Y. Zhang, *Adv. Mater.*, 2020, **32**, e1906225.
3 J. Chen, J. S. Wei, P. Zhang, X. Q. Niu, W. Zhao, Z. Y. Zhu, H. Ding and H. M. Xiong, *ACS Appl. Mater. Interfaces*, 2017, **9**, 18429–18433.
4 Z. Ma, J. Zhou, J. Zhang, S. Zeng, H. Zhou, A. T. Smith, W. Wang, L. Sun and Z. Wang, *Mater. Horiz.*, 2019, **6**, 2003–2008.
5 B. Lee, J. Y. Oh, H. Cho, C. W. Joo, H. Yoon, S. Jeong, E. Oh, J. Byun, H. Kim, S. Lee, J. Seo, C. W. Park, S. Choi, N. M. Park, S. Y. Kang, C. S. Hwang, S. D. Ahn, J. I. Lee and Y. Hong, *Nat. Commun.*, 2020, **11**, 663.
6 Y. Wang, J. Wang, Q. Ma, Z. Li and Q. Yuan, *Nano Res.*, 2018, **11**, 5499–5518.
7 Y. J. Kim, H. S. Jung, J. Lim, S. J. Ryu and J. K. Lee, *Langmuir*, 2016, **32**, 8077–8083.
8 M. Wang, D. Shen, Z. Zhu, J. Ju, J. Wu, Y. Zhu, M. Li, C. Yuan and C. Mao, *Mater. Today Adv.*, 2020, **8**, 100113.
9 D. Tian, Z. Zhu, L. Xu, H. Cong and J. Zhu, *Mater. Horiz.*, 2019, **6**, 1215–1221.
10 S. Lin, H. Lin, C. Ma, Y. Cheng, S. Ye, F. Lin, R. Li, J. Xu and Y. Wang, *Light: Sci. Appl.*, 2020, **9**, 22.
11 S. Zheng, J. Shi, X. Fu, C. Wang, X. Sun, C. Chen, Y. Zhuang, X. Zou, Y. Li and H. Zhang, *Nanoscale*, 2020, **12**, 14037–14046.
12 J. Yang, Y. Liu, Y. Zhao, Z. Gong, M. Zhang, D. Yan, H. Zhu, C. Liu, C. Xu and H. Zhang, *Chem. Mater.*, 2017, **29**, 8119–8131.
13 Y. Zhuang, L. Wang, Y. Lv, T.-L. Zhou and R.-J. Xie, *Adv. Funct. Mater.*, 2018, **28**, 1705769.
14 Y. Zhuang, Y. Lv, L. Wang, W. Chen, T. L. Zhou, T. Takeda, N. Hirosaki and R. J. Xie, *ACS Appl. Mater. Interfaces*, 2018, **10**, 1854–1864.
15 R. R. Petit, S. E. Michels, A. Feng and P. F. Smet, *Light: Sci. Appl.*, 2019, **8**, 124.
16 F. Liu, W. Yan, Y. J. Chuang, Z. Zhen, J. Xie and Z. Pan, *Sci. Rep.*, 2013, **3**, 1554.
17 L. Song, P.-P. Li, W. Yang, X.-H. Lin, H. Liang, X.-F. Chen, G. Liu, J. Li and H.-H. Yang, *Adv. Funct. Mater.*, 2018, **28**, 1707496.
18 J. Du, A. Feng and D. Poelman, *Laser Photonics Rev.*, 2020, **14**, 2000060.
19 J. Jin, H. Jiang, Q. Yang, L. Tang, Y. Tao, Y. Li, R. Chen, C. Zheng, Q. Fan, K. Y. Zhang, Q. Zhao and W. Huang, *Nat. Commun.*, 2020, **11**, 842.
20 C. Liu, Z. Xia, M. Chen, M. S. Molokeev and Q. Liu, *Inorg. Chem.*, 2015, **54**, 1876–1882.
21 M. Back, E. Trave, J. Ueda and S. Tanabe, *Chem. Mater.*, 2016, **28**, 8347–8356.

22 M. Back, J. Ueda, M. G. Brik, T. Lesniewski, M. Grinberg and S. Tanabe, *ACS Appl. Mater. Interfaces*, 2018, **10**, 41512–41524.
23 Y. Zhang, R. Huang, H. Li, Z. Lin, D. Hou, Y. Guo, J. Song, C. Song, Z. Lin, W. Zhang, J. Wang, P. K. Chu and C. Zhu, *Small*, 2020, **16**, e2003121.
24 O. Taktak, H. Souissi and S. Kammoun, *J. Lumin.*, 2020, **228**, 117563.
25 D. Chen, X. Chen, X. Li, H. Guo, S. Liu and X. J. O. L. Li, *Opt. Lett.*, 2017, **42**, 4950–4953.
26 B. del Rosal, E. Ximendes, U. Rocha and D. Jaque, *Adv. Opt. Mater.*, 2017, **5**, 1600508.
27 S. Wang, S. Ma, G. Zhang, Z. Ye and X. Cheng, *ACS Appl. Mater. Interfaces*, 2019, **11**, 42330–42338.
28 Y. Katayama, T. Kayumi, J. Ueda, P. Dorenbos, B. Viana and S. Tanabe, *J. Mater. Chem. C*, 2017, **5**, 8893–8900.
29 Y. Katayama, T. Kayumi, J. Ueda and S. Tanabe, *Opt. Mater.*, 2018, **79**, 147–151.
30 J. Xu and S. Tanabe, *J. Lumin.*, 2019, **205**, 581–620.
31 Y. Zhang, R. Huang, H. Li, D. Hou, Z. Lin, J. Song, Y. Guo, H. Lin, C. Song, Z. Lin and J. Robertson, *Acta Mater.*, 2018, **155**, 214–221.
32 Z. Pan, Y. Y. Lu and F. Liu, *Nat. Mater.*, 2012, **11**, 58–63.
33 Y. Katayama, B. Viana, D. Gourier, J. Xu and S. Tanabe, *Opt. Mater. Express*, 2016, **6**, 1405.
34 D. Dai, Z. Wang, C. Liu, X. Li, L. Zhang, Z. Xing, Z. Yang and P. Li, *ACS Appl. Electron. Mater.*, 2019, **1**, 2551–2559.
35 J. Xu, D. Murata, J. Ueda, B. Viana and S. Tanabe, *Inorg. Chem.*, 2018, **57**, 5194–5203.
36 X. Chen, W. Xu, L. Zhang, X. Bai, S. Cui, D. Zhou, Z. Yin, H. Song and D.-H. Kim, *Adv. Funct. Mater.*, 2015, **25**, 5462–5471.
37 R. S. Li, J. H. Liu, T. Yang, P. F. Gao, J. Wang, H. Liu, S. J. Zhen, Y. F. Li and C. Z. Huang, *Anal. Chem.*, 2019, **91**, 11185–11191.
38 J. Wang, T. Wei, X. Li, B. Zhang, J. Wang, C. Huang and Q. Yuan, *Angew. Chem., Int. Ed.*, 2014, **53**, 1616–1620.